ROADWAY SAFETY INSTITUTE

Human-centered solutions to advanced roadway safety

Characterizing Phase-Center Motion of GNSS Antennas Used in High-Accuracy Positioning

Aditya Dave
Robert Sainati
Rhonda Franklin

Department of Electrical and Computer Engineering
University of Minnesota

Ricardo Saborio
Kerry Sun
Demoz Gebre-Egziaher

Department of Aerospace Engineering and Mechanics
University of Minnesota

Final Report

CTS 19-17

University of Minnesota Driven to Discover℠
The University of Akron
Illinois University of Illinois at Urbana-Champaign
Southern Illinois University Edwardsville
Western Michigan University

Technical Report Documentation Page

1. Report No.	2.	3. Recipients Accession No.	
CTS 19-17			
4. Title and Subtitle Characterizing Phase-Center Motion of GNSS Antennas Used in High-Accuracy Positioning		5. Report Date June 2019 6.	
7. Author(s) Aditya Dave[1], Ricardo Saborio[2], Kerry Sun[2], Robert Sainati[1], Demoz Gebre-Egziaher[2] and Rhonda Franklin[1]		8. Performing Organization Report No.	
9. Performing Organization Name and Address [1]Department of Electrical and Computer Engineering University of Minnesota 4-174 Keller Hall 200 Union Street SE, Minneapolis, MN 55455 [2]Department of Aerospace Engineering and Mechanics University of Minnesota 107 Akerman Hall 110 Union Street SE, Minneapolis, MN 55455		10. Project/Task/Work Unit No. CTS# 2018054 11. Contract (C) or Grant (G) No. DTRT13-G-UTC35	
12. Sponsoring Organization Name and Address Roadway Safety Institute Center for Transportation Studies University of Minnesota University Office Plaza, Suite 440 2221 University Ave SE Minneapolis, MN 55414		13. Type of Report and Period Covered Final (May 2018 to May 2019) 14. Sponsoring Agency Code	
15. Supplementary Notes http://www.roadwaysafety.umn.edu/publications/			

16. Abstract (Limit: 250 words)

Emerging transportation applications require positioning solutions with accuracy of a few centimeters. Current Global Navigation Satellite Systems (GNSS), such as GPS, GLONASS, and Galileo are, in some instances, capable of providing this level of accuracy. Real-Time Kinematic (RTK) techniques can generate solutions accurate to a few centimeters in a given locale. Precise Point Positioning (PPP) techniques promise to deliver RTK-level performance on a global scale. Even though low-cost, RTK-capable GNSS receivers are available today, antennas are a key component affecting quality of the positioning solution. Unless coupled with a high-quality (thus, more expensive) antenna, a low-cost receiver may not provide the centimeter-level accuracy needed for a safety-critical transportation application (e.g., autonomous vehicle, driver assist systems, etc.). Stability of the antenna phase-center is dependent on the antenna quality and can potentially move on the order of tens of mm if not centimeters. The purpose of the work reported here was to characterize the nature of this motion as a function of antenna quality. Anechoic chamber tests were performed using one high-cost and another low-cost GNSS antenna. The selected antennas represented “book ends” on the cost spectrum. These experiments showed that phase-center motion on the low-cost antenna can be a factor of four times larger than on high-quality antennas. Since anechoic chamber tests are not practical for each antenna installation in transportation applications, methods for antenna-specific, *in-situ*, phase-center motion calibration (modelling) methods have been suggested. Preliminary results suggested efficacy of these *in-situ* methods.

17. Document Analysis/Descriptors	18. Availability Statement		
Global Positioning System, Satellite navigation systems, Antennas, Testing	No restrictions. Document available from: National Technical Information Services, Alexandria, Virginia 22312		
19. Security Class (this report)	20. Security Class (this page)	21. No. of Pages	22. Price
Unclassified	Unclassified	37	

Characterizing Phase-Center Motion of GNSS Antennas used in High Accuracy Positioning Applications

FINAL REPORT

Prepared by:

Aditya Dave
Robert Sainati
Rhonda Franklin

Dept. of Electrical and Computer Engineering
University of Minnesota

Ricardo Saborio
Kerry Sun
Demoz Gebre-Egziabher

Dept. of Aerospace Engineering
University of Minnesota

June 2019

Published by:

Roadway Safety Institute
Center for Transportation Studies
University of Minnesota
University Office Plaza, Suite 440
2221 University Ave SE
Minneapolis, MN 55414

ACKNOWLEDGMENTS

The funding for this project was provided by the United States Department of Transportation's Office of the Assistant Secretary for Research and Technology for the Roadway Safety Institute, the University Transportation Center for USDOT Region 5 under the Moving Ahead for Progress in the 21st Century Act (MAP-21) federal transportation bill passed in 2012.

TABLE OF CONTENTS

LIST OF FIGURES

LIST OF TABLES

EXECUTIVE SUMMARY

Emerging transportation applications require positioning solutions with accuracy of a few centimeters. Current Global Navigation Satellite Systems (GNSS), such as GPS, GLONASS, and Galileo are, in some instances, capable of providing this level of accuracy. Real-Time Kinematic (RTK) techniques can generate solutions accurate to a few centimeters in a given locale and precise Point Positioning (PPP) techniques promise to deliver RTK-level performance on a global scale. Even though low-cost, RTK-capable GNSS receivers are available today, consistent, centimeter-level accuracy requires well-calibrated antennas. Antenna systems are a key component of the overall system and affect the quality of the positioning solution achieved. Thus, unless they are coupled with a high-quality (thus, more expensive) antenna system, low-cost receivers may not provide the centimeter-level accuracy needed by a safety-critical transportation application (e.g., autonomous vehicle, driver assist systems, etc.). One key calibration parameter is the antenna's phase-center; the hypothetical point on the antenna where it is assumed that the GNSS range or carrier phase measurements are being made. Antennas used in survey applications can be tens of centimeters in diameter, and as such, if the phase-center's location is not known precisely on the antenna, a few centimeters worth of positioning errors can be introduced.

Estimating the location of the phase-center is a challenging problem because it is difficult to isolate it from other antenna measurement errors. In other words, antenna phase-center errors are unobservable (using the language of estimation theory) from other errors. For example, some GNSS antenna systems exhibit error characteristics that are functions of the geometry of the line-of-sight vector to the GNSS satellites. That is, the phase measurement error (differential or stand-alone) for signals originating from a satellite, with a low elevation angle will be different from one having a high-elevation angle. There can be a similar dependence on azimuth angle as well. Simply put, the phase error of an antenna system may not be isotropic with respect to azimuth and elevation angles of the line-of-sight vector between it and the GNSS satellites. This leads to an apparent motion of the antenna phase-center, referred to as *phase-center stability* in this report. Stability of the antenna phase-center is dependent on the antenna quality.

The purpose of the work reported here is to characterize the nature of this phase-center motion as a function of antenna quality and, if possible, develop a mathematical model for it that can be used to improve RTK and PPP solutions. To this end, anechoic chamber tests are performed using one high-cost and another low-cost GNSS antenna. The selected antennas represent "book ends" on the cost spectrum. These experiments show that phase-center motion can be as large as 3.5 cm on high-quality (survey grade) antennas but is limited to the plane of the antenna system. Phase-center motion can be much larger for the low-cost antennas and is not limited to the plane of the antenna system—the motion can be a three dimensional "ball" in space. Since phase-center motion is a function of the antenna system (antenna, ground plane, connectors, cables), anechoic chamber characterization may not capture the behavior seen when the antenna is installed and used on a vehicle. Anechoic chamber characterization is not practical for each antenna installation in a vehicle. This suggests that it may be beneficial to develop methods for antenna-specific, *in-situ*, phase-center motion calibration (modelling) methods. Accordingly, we present preliminary results, which suggest approaches that can be used to develop such *in-situ* phase-center calibration.

CHAPTER 1: OVERVIEW

Global Navigation Satellite Systems (GNSS) is a term used to collectively describe satellite-based positioning and timing systems of which GPS (operated by the United States government) and GLONASS (operated by the Russian Federation) are the most widely used systems today. The European Union's Galileo is the newest, fully operational GNSS and its number of users is increasing every day. It will be followed soon by China's GNSS known as Beidou. The sub-meter accuracy provided by GNSS has revolutionized road, rail, air, and marine transportation systems worldwide. GNSS timing functions are routinely used to discipline oscillators and, as such, have become the *de-facto* heartbeat for the modern, interconnected world.

GNSS receivers are capable of generating a positioning solution that is accurate to a few centimeters using a signal processing approach called *Real-Time Kinematic* (RTK) processing. RTK provides an accurate timing and positioning solution in a local geographic area and has been used by surveyors for over a decade. An emerging technique known as *Precise Point Positioning* (PPP) promises to deliver RTK-level accuracy but with a global coverage. Currently, inexpensive and compact GNSS receivers capable of producing RTK and potentially PPP solutions are available on the market.

The ability of RTK and PPP techniques to generate a centimeter-level accurate position solution in real-time, using a compact and inexpensive receiver, will be an enabler of many novel, efficient and safety enhancing automotive features. For example, it will enable lane departure warning systems to be ubiquitous as demonstrated, for example, by General Motors in its newer vehicles. It can also be the basis for advanced driver assistive systems in snowplows and similar operations.

At the heart of both RTK and PPP is the ability to precisely model and remove the effect of errors that degrade the quality of the GNSS signal processed by a receiver. This is essentially a calibration operation whereby various errors are eliminated from the GNSS signal before it is used for generating a positioning and timing solution. RTK leverages the fact that many of the errors affecting the received GNSS signal are either channel errors that can be estimated by the receiver itself (e.g., ionosphere delay) or *common-mode* errors that can be eliminated by a network of external receivers (e.g., troposphere, satellite clock, satellite ephemeris) in communication with the user. However, there are some errors that are receiver-specific. One of these errors that is unique to each user is the antenna phase error. As things stand currently, antenna phase error is modeled by the manufacturers of the antenna (or receiver) *a priori*. This is not a trivial process and it requires extensive infrastructure (e.g., an anechoic chamber). As such, it results in an increased cost of antennas used for precise GNSS positioning. However, if these errors can be estimated in-service, then there is a possibility of reducing the cost of high-precision GNSS receiver/antenna systems.

The purpose of this work was to take the first steps in assessing whether antenna phase errors can be estimated *in-situ* rather than *a priori* by the manufacturers. To this end, the work described in this report was organized around the following objectives:

Objective #1: Demonstrate how the phase-center for a GNSS antenna can be determined experimentally

Objective #2: Characterize the errors associated with locating the antenna phase-center for high- and low-quality GNSS antennas

Objective #3: Suggest a framework for estimating phase-center location from measurements of GNSS carrier phase observables

This is accomplished by a series of anechoic chamber and field experiments using a pair of GPS antennas. These antennas are representative of a high-quality and a low-quality antenna, thereby spanning the spectrum of performance. Accordingly, the remainder of this report is organized as follows:

- In Chapter 2, we provide an overview of high-accuracy GNSS positioning techniques. This is not supposed to be a tutorial on the subject but rather a description that will allow putting the rest of the material in the report in context.
- In Chapter 3, anechoic chamber tests to characterize antenna errors for a pair of GNSS antennas is described. The purpose of this experiment is to characterize antenna phase-center motion errors.
- In Chapter 4, we provide a summary and conclusion as well as suggestions for future work to develop *in-situ* calibration of antenna phase-center motion. We do this by collecting GNSS data, which can be used to correlate error behavior seen in the anechoic chamber and observed by a GNSS receiver in the field. The challenges of fitting an error model to the observed phase error are described.

CHAPTER 2: GNSS HIGH ACCURACY POSITIONING

We will use the term high-accuracy GNSS in the report to collectively describe the techniques of Real Time Kinematic (RTK) and Precise Point Positioning (PPP). Both of these techniques provide a way in which centimeter level positioning accuracy can be obtained using GNSS. Both methods, in part, remove common mode errors from the GNSS signal-in-space by using information derived from a network of GNSS receivers. In the work described in this report, our interest is in the non-common mode errors introduced by the design of the antenna system itself. Thus, without a loss of generality we will focus on RTK. However, our findings are equally applicable to PPP techniques.

The remainder of this chapter is organized as follows: First we will discuss basics of the RTK solution. Next, we describe how errors associated with the antenna system impact the final RTK solution. As noted in Chapter 1, this is not supposed to be a tutorial on the subject but rather a description that will allow putting the rest of the material in the report in context. A more detailed treatment of this material can be found in texts on GNSS such as [1].

$$\lambda\phi = \lambda(\text{Integer Number of Cycles (N)} + \text{Fractional Cycles})$$

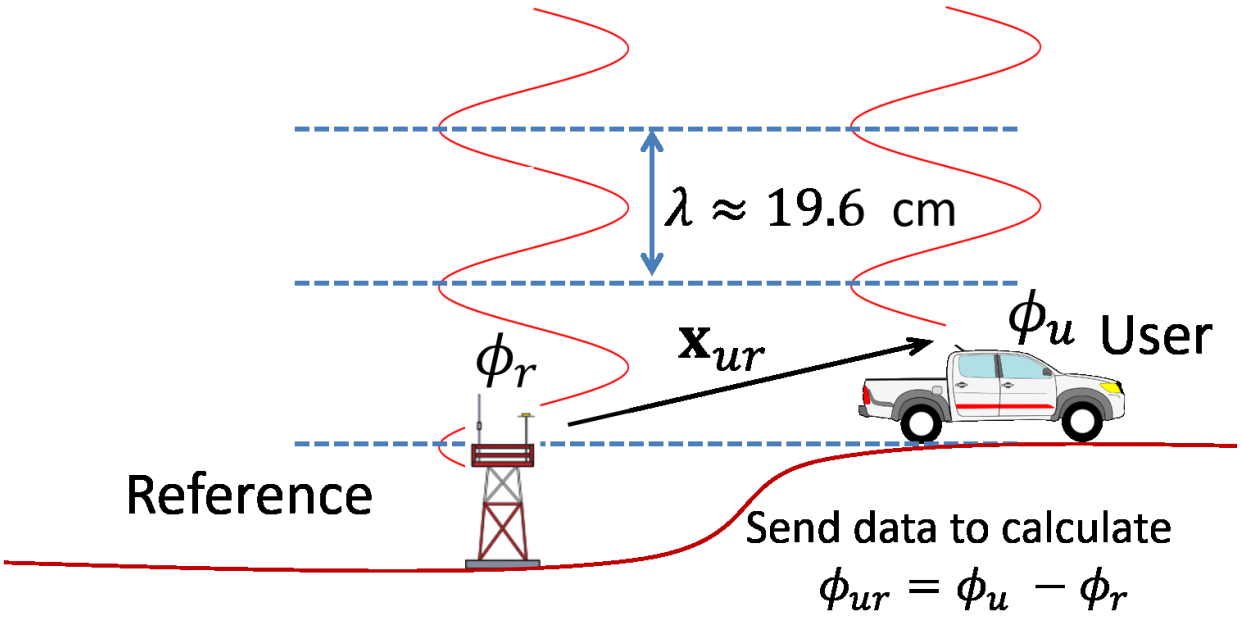

Figure 2.1 Schematic showing the basics of RTK positioning

2.1 REAL TIME KINEMATIC (RTK) GNSS

Fig 2.1 shows an idealized setup of a RTK system. In this case the user is located at $\mathbf{x}_u$ and the reference receiver is located at $\mathbf{x}_r$. If we assume that $\mathbf{x}_r$ is precisely known (or the uncertainty in it is small), then the RTK problem is that of determining the baseline vector $\mathbf{x}_{ur} = \mathbf{x}_u - \mathbf{x}_r$. The carrier phase measurement made by the user receiver located at position $\mathbf{x}_u$ which is being transmitted by satellite k is given by [1] [2] [3] :

$$\varphi_u^{(k)}(t) = \frac{1}{\lambda}\left[r_u^{(k)} + I_\varphi + T_\varphi\right] + \frac{c}{\lambda}\left(\delta t_u(t) - \delta t^k(t-\tau)\right) + N + \varepsilon_u^{(k)}$$

where $\phi_u^{(k)}$ is the carrier phase measurement from the k[th] GNSS satellite; λ is the signals wave length; c is the speed of light; $r_u^{(k)}$ is the geometric range between the user and the GNSS satellite; I_φ is the ionospheric delay in the transmitted signal; T_φ is the tropospheric delay; in the transmitted signal; δt_u is the user clock bias; δt^k is the satellite clock bias; N is the carrier cycle integer ambiguity; and $\varepsilon_u^{(k)}$ are the un-modeled measurement errors which include any errors introduced by the antenna systems. A similar equation for the measurements made by the reference receiver can be written where the subscript u are replaced by r.

If the reference receiver and the user are geometrically close (a few kilometers apart), then the ionosphere and troposphere errors will be common-mode error for a given GNSS satellite. The satellite clock error will also be a common-mode error. Thus, taking the difference between user and reference measurements yields the following system of equations:

$$\begin{bmatrix} \varphi_{ur}^{(1)} \\ \varphi_{ur}^{(2)} \\ \vdots \\ \varphi_{ur}^{(K)} \end{bmatrix} = \lambda^{-1}\begin{bmatrix} \left(-\mathbf{1}_r^{(1)}\right)^T \\ \left(-\mathbf{1}_r^{(2)}\right)^T \\ \vdots \\ \left(-\mathbf{1}_r^{(K)}\right)^T \end{bmatrix}\mathbf{x}_{ur} + \frac{c}{\lambda}\delta t_{ur}\begin{bmatrix} 1 \\ 1 \\ \vdots \\ 1 \end{bmatrix} + \begin{bmatrix} N_{ur}^{(1)} \\ N_{ur}^{(2)} \\ \vdots \\ N_{ur}^{(K)} \end{bmatrix} + \begin{bmatrix} \varepsilon_{\varphi,ur}^{(1)} \\ \varepsilon_{\varphi,ur}^{(2)} \\ \vdots \\ \varepsilon_{\varphi,ur}^{(K)} \end{bmatrix}$$

The variable $\varphi_{ur} = \varphi_u - \varphi_r$ is called the single difference (SD) and the equation above is the single difference measurement equation. The variable $\left(-\mathbf{1}_r^{(k)}\right)$ is the line of sight vector from the reference receiver to the k[th] GNSS satellite. This equation can be written in a more compact form using matrix/vector notation as follows:

$$\Delta\boldsymbol{\varphi}_{ur} = \mathbf{G}_s\mathbf{x}_{ur} + \mathbf{b}_{ur} + \mathbf{N}_{ur} + \boldsymbol{\varepsilon}_{ur}$$

The last term in the equation, $\boldsymbol{\varepsilon}_{ur}$, is the SD measurement noise. The key take away from this equation is that a SD results in un-modeled errors which, among other things, includes a sum of the two antenna

system errors (user and reference). As we will show in the next chapter, this error term has at least three (if not more) components:

$$\boldsymbol{\varepsilon}_{ur} = \boldsymbol{\varepsilon}_{ur,p} + \boldsymbol{\varepsilon}_{ur,a} + \boldsymbol{\varepsilon}_{ur,n}$$

The first term in the equation above, $\boldsymbol{\varepsilon}_{ur,p}$, represent errors due to the phase-center motion. The second term, $\boldsymbol{\varepsilon}_{ur,a}$, are error due to non-isotropy of the antenna gain pattern. The third term, $\boldsymbol{\varepsilon}_{ur,n}$ is uncorrelated noise or the residual left over after all other errors have been calibrated.

When RTK is used in practice, we normally implement a double difference (DD) formulation. In this case, one GNSS satellite is used a reference. Then and all the single difference measurements from the other satellites are subtracted from the reference satellites measurement to yield the following system of equations:

$$\begin{bmatrix} \varphi_{ur}^{(21)} \\ \varphi_{ur}^{(31)} \\ \vdots \\ \varphi_{ur}^{(K1)} \end{bmatrix} = \lambda^{-1} \begin{bmatrix} -\left(\mathbf{1}_r^{(2)} - \mathbf{1}_r^{(1)}\right)^T \\ -\left(\mathbf{1}_r^{(3)} - \mathbf{1}_r^{(1)}\right)^T \\ \vdots \\ -\left(\mathbf{1}_r^{(K)} - \mathbf{1}_r^{(1)}\right)^T \end{bmatrix} \mathbf{x}_{ur} + \begin{bmatrix} N_{ur}^{(21)} \\ N_{ur}^{(31)} \\ \vdots \\ N_{ur}^{(K1)} \end{bmatrix} + \begin{bmatrix} \varepsilon_{\varphi,ur}^{(21)} \\ \varepsilon_{\varphi,ur}^{(31)} \\ \vdots \\ \varepsilon_{\varphi,ur}^{(K1)} \end{bmatrix}$$

In the equation above, satellite #1 has been used as the reference relative to which all other satellite measurements are differenced. Notice that this removes the clock bias term. The significance of this will be discussed in Chapter 4. Once again, using matrix/vector notation this equation can be written in the following compact form:

$$\Delta\boldsymbol{\varphi}_{ur}^{kl} = \mathbf{G}_d \mathbf{x}_{ur} + \mathbf{N}_{ur}^{kl} + \boldsymbol{\varepsilon}_{ur}^{kl}$$

Once again the key point that needs to be emphasized is this: the measurement error is not necessarily uncorrelated noise but will include systematic errors from the antenna system.

2.2 IMPACT OF AND MITIGATING ANTENNA ERRORS

As we will show in the next chapter, un-calibrated antenna errors can be on the order of a few centimeters. Thus, left uncalibrated they can impact the ability to obtain errors that are on the order of a few centimeters. Furthermore, if left uncalibrated they impact the ability to fix integer ambiguities rapidly. In the next chapter we will show the size of these errors and suggest potential approaches for calibrating them *in-situ*.

CHAPTER 3: EXPERIMENTAL DETERMINATION OF ANTENNA PHASE-CENTER

In Chapter 2, we described the various errors that contribute to positioning and timing uncertainty in RTK/PPP GNSS solutions. In this chapter we describe experiments conducted to characterize antenna phase-center errors and characterize its motion. To this end, measurements were performed to identify the phase-center location for two types of GNSS antennas. For these measurements, the GNSS receive antennas are mounted on a stand and placed in an anechoic chamber to determine the phase-center behavior.

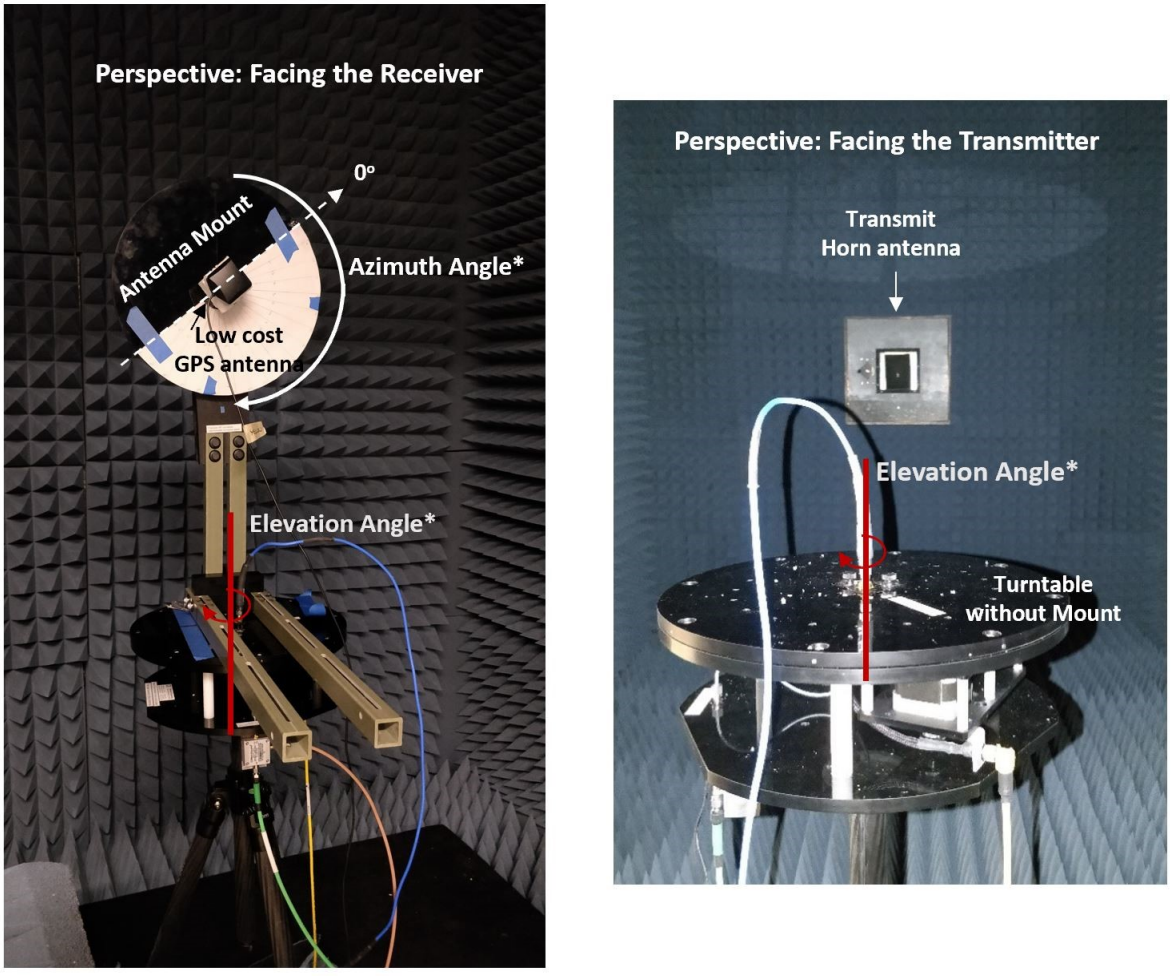

***Elevation Angle = the rotation axis of the turn table.**

Figure 3.1 Anechoic chamber setup used for the phase-center motion characterization described in Chapter 3

The two antenna used in these tests (representing the "book ends" of a high- and low-cost antennas) were the NAVCOM ANT-3001R [4] and the u-Blox ANN-MS [5]. The experimental setup used is shown in Fig 3.1. In the laboratory measurement setting, each antenna is mounted on a stand that faces a horn-antenna to simulate the transmission from a GNSS satellite. The antenna signal radiates in the z-direction toward the transmitter and the antenna structure is located in the x-y plane. A transmission measurement

is obtained that contains magnitude and phase information. Phase-center is defined as the point where electromagnetic radiation spreads outward with the signal being equal from any point on the sphere [2], [3], [6] .

In theory, the phase-center should be a fixed point on the antenna. As such, if a GNSS antenna is rotated about its phase-center (i.e., the phase-center is fixed in space), no change in the phase and[1] pseudo-range measurements should be observed. The experimental method devised here to determine the phase-center exploits this fact. The approach used to characterize the phase-center location in this work in an anechoic chamber is the following: A GNSS antenna is mounted as shown in Fig. 3.1. For a given measurement, this receive antenna translated in the x, y, and z plane for a given rotation angle in the x-y plane until the phase variation of the received signal (from a transmit horn antenna) is constant (invariant). Both elevation angle and azimuth angles indicated in Fig. 3.1 are incremented in steps to cover 180 degrees. The azimuth angle changes from 0 degrees to 180 degrees in steps of 10 degrees. 0 degrees position is referred to the case when the connector points downwards. The elevation angle changes from 0 degrees to 180 degrees in increment of 2 degrees. Elevation of 90 degrees indicates boresight orientation of the receiver, i.e. the receive antenna faces the transmit horn antenna.

Ideally, a circularly polarized transmit antenna would be used in the test to match GNSS antenna polarization. In this work however, linearly polarized horn antennas were used. To capture the effect of circular polarization, two measurements were performed with orthogonal polarization to determine the phase-center location in terms of x, y, and z coordinates. Orthogonal polarization is achieved by collecting data from the transmit antenna at its reference orientation and at 90 degree rotation from its reference orientation. Since the horn antenna used is rectangular, its long side is oriented along either the x or y direction.

The determined phase-center applies to a specific orientation angle of the GNSS antenna with respect to the horn antenna and its rotation axis. The GNSS antenna is then rotated about an axis perpendicular to it to determine the phase-center in that orientation. By repeating this process, a set of phase-centers are determined for all the orientation angles of the antenna.

It should be noted that this approach has one key limitation. If there are errors that are dependent on the direction of arrival of the signal, then they will become indistinguishable from phase-center motion errors. Any anisotropy in phase error pattern of the antenna will lead to phase-center motion being confounded with other errors. Therefore, the phase-center location estimated by this approach will be the average phase-center location which includes motion due to other confounding effects.

[1] Even though the term “phase” is used to describe this measurement, a more accurate description would be *accumulated Doppler* (or ADR) which is the integral of the Doppler shift in the signal. Thus, the ADR represents a second range measurement with an unknown initial condition.

3.1 EXPERIMENTAL SETUP

In what follows we will use the tests performed to characterize the phase-center variation for two antennas. The antenna was rotated about two axes. One is the axis of the turn table (y-axis) and other is the axis that lies perpendicular to the turn table (z-axis) and lies along the boresight direction of the antenna. Fig 3.1 shows both the axes relative to the high cost and low cost antenna.

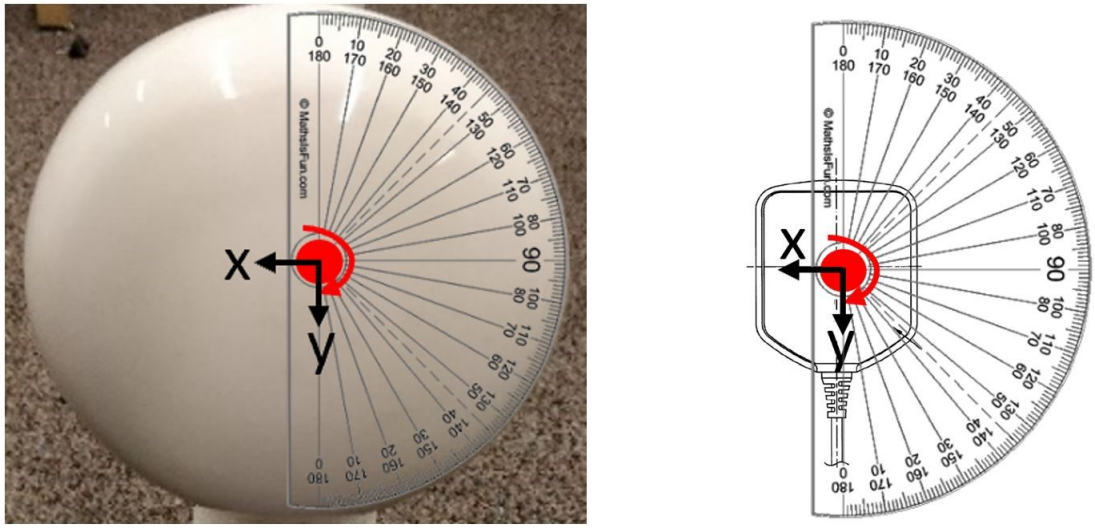

(a) (b)

Figure 3.2 Azimuth and elevation angle sweep directions with respect to the antenna. (a) High-cost Navcom antenna. (b) Low-cost Ublox antenna

3.2 THEORY OF MEASUREMENTS

This section details the transmission coefficient measurement method used to determine phase-center. The interpretation of the antenna measurements and their relation to the locational accuracy is obtained from two different GNSS antenna.

1. Each GNSS antenna is measured in an anechoic chamber for isolation. A transmission measurement, also referred to S21, is obtained that behaves like a "transfer" function. The transfer function relates the received signal to the incident signal. In our work, the transmit antenna representing the satellite is a horn antenna and the receive antenna is the GNSS antenna.
2. The S21 measurement obtained in the anechoic chamber uses a 2-port vector network analyzer (VNA) to provide the source signal (port 1) and to accept the receive signal (port 2). The measurement reference plane is located at the face of the VNA. Therefore, the S21 measurements consist of input and output cables to the source horn antenna and GNSS antenna, the air channel between the two antennas, and all associated external circuitry between the output of the GNSS antenna system and

receive port to the VNA. The S21 measurement is a calibrated measurement. The path loss between the transmit and receive antennas for the reference calibration made using horn antennas is 32dB. The peak gain[2] for the high cost circularly polarized antenna system (antenna + amplifiers) according to the datasheet is 39dBiC [4] and the low cost antenna system is 32dBiC [5]. The gain obtained in the measurements after including the calibrated path loss value is 36dBi for the high cost antenna and 29dBi for the low cost antenna system. The loss of 3dBi is due to the use of linearly polarized horn antennas sending signals to the circularly polarized receivers.

3. In this work, the GNSS antenna system is the Antenna System under Test (ASUT). This ASUT is a one-port physical structure that includes an antenna plus any circuitry between the antenna and the external RF connector that serves as the access point for the output signal of the AUT. The circuitry within the ASUT system usually has a device (quadrature hybrid or similar structure) along with the actual antenna structure that forms a circularly polarized antenna. The polarization sense is matched to the incoming GNSS satellite signal. There is also typically a low noise amplifier to improve system sensitivity. The S21 measurements, therefore, are for the GNSS antenna system and not just the GNSS antenna.

   The S21 measurements in this work are done with a linear polarization. For a fixed antenna orientation, two measurements were performed using two spatially orthogonal polarizations (i.e. vertical and horizontal). Each measurement represents the response of the ASUT as a function of angle in the plane of rotation. For a 10˚ resolution of angles in the x-y plane indicated in Fig. 3.2, a sweep to 180˚ in x-z plane is made for both orthogonal polarizations. The sweep ranges from -90˚ to 90˚ with 0˚ being boresight.

4. GNSS signals are circularly polarized. The horn in our anechoic measurement that represents the GNSS source signal is linearly polarized and the GNSS antenna system (including antenna, hybrid, amplifier, etc.) is circularly polarized but is a linear system. In most cases, the GNSS antenna has two ports; one for each of the two orthogonal E fields of the circularly polarized GNSS signal. The signals from the two antenna ports serve as inputs to a quadrature hybrid (or other similar device) that combines the two signals to create the "GNSS signal" that is delivered to the GNSS receiver for processing. For the real GNSS signal, the signals coming out of the antenna ports will be of equal magnitude but with a phase shift between them of -90^o (which one is phase shifted depends upon the "handedness" of the GNSS circularly polarized signal). This phase shift is produced by the GNSS satellite antenna when transmitting to create a circularly polarized signal. The hybrid "reverses" the phase shift of shifted port signal so that it adds to the other port signal thereby maximizing the response.

   Therefore, to represent the satellite to GNSS receive antenna scenario accurately, we obtain S21 measurements over the angle range of -90^o to 90^o at one of the angles of rotation for two polarizations (obtained by proper orientation of the horn) since the horn and the GNSS receive antenna are in fixed

[2] http://radiomobile.pe1mew.nl/?The_program:Definitions:dBiC

location in our measurement set-up. The S21 obtained when the horn is oriented to produce "vertical" (i.e. with respect to the anechoic chamber floor) polarization is the GNSS antenna system response for one of the E field components of a GNSS signal incident in the plane defined by the angle of rotation (e.g. 0^o, 10^o, etc.). Likewise, the S21 measured when the horn is rotated 90^o to produce "horizontal" polarization represents the antenna system response to the other (orthogonal) E field component of a GNSS incident in the same plane (as denoted by the angle of rotation).

Since there is no change other than a physical rotation of the horn antenna for these two measurements, there is no phase shift between the "vertical" and "horizontal" incident horn fields. As mentioned earlier, the hybrid combines the two signals and to maximize the response, one signal must be phase shifted by 90^o. For the actual GNSS signal there will be a -90^o between them. So to replicate the antenna system response to a GNSS signal, a phase shift of -90^o needs to be added to the S21 for one of the measurements at a given angle of rotation. This addition mimics the phase shift present in the GNSS signal. Since the antenna system is linear, we can add the two S21 responses to get the overall response. When the two measurements are added with the inclusion of a phase shift of -90 degrees by one of the measurements to reflect the phase shift between the orthogonal field components in the GNSS then the antenna response to a GNSS signal is obtained. This combined S21 data shows how the received signal amplitude and phase would vary as the satellite passes over at a fixed angle of rotation.

5. Ideally, the response obtained by appropriately adding the two S21 measurement assumes the reference point for the antenna location is at its phase-center. The measurements, however, indicate that the phase-center is not necessarily at the mounting point of the antenna (or another possible reference point such as the physical center). The antenna response, therefore, needs to include the error induced by the actual difference between the assumed reference point and the actual phase-center location.

3.3 DATA ANALYSIS

The rotation along the z-axis, shown in Fig 3.2, represents the azimuth angle change. The azimuth angle change is the rotation in the x-y plane with a resolution of 10° as described in point 4 of the previous section and Fig. 3.2. The rotation in the x-z plane represents change in elevation angle. For each azimuth angle, the antenna, the elevation angle is swept from -90 degrees to 90 degrees in increments of two degrees. The azimuth angle is then incremented by 10 degrees and then the measurement is repeated. The measurements are made for both vertical and horizontal linear polarizations transmitted using a horn antenna. Horizontal linear polarization is when the long side of the horn is vertical; the vertical linear polarization is when the long side is in the horizontal direction. The position where the change in S21 phase is minimal is designated as the phase-center. This position is represented by two coordinates. They are different for each polarization and angle. Theory states that if for one of the polarizations, the coordinates obtained are 'x' and 'z' then for the other polarization, the co-ordinates obtained would be 'y' and 'z'. This is because both polarizations are orthogonal to each other. If the 'z' coordinate for both measurements is different, an average of both values is taken. The co-ordinate system for both the antennas is shown in Fig. 3.3.

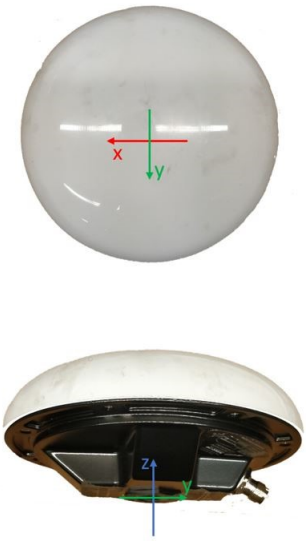

(a)

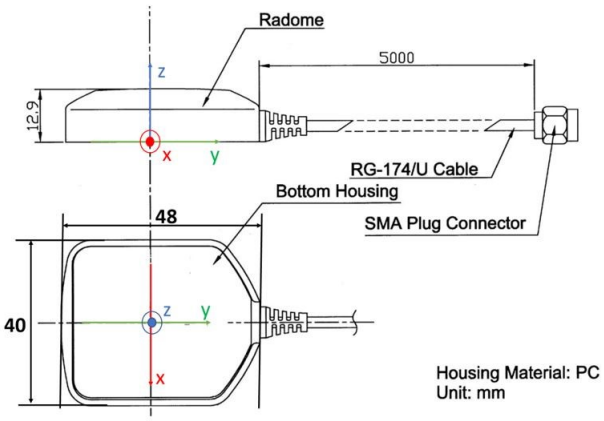

(b)

Figure 3.3 The reference co-ordinate system for both the antennas. (a) High-cost antenna top view and side view and (b) Low-cost antenna side view and top view

For the GNSS antennas, we assume we are working with GPS. Thus, at the L1 frequency, the wavelength is approximately 20 cm. For a sub-centimeter level accuracy, the phase variation should be less than (360/20) = 18 degrees. If the variation of the S21 phase is within 18 degrees for all elevation angles, the point of rotation corresponding to that measurement is designated as the phase-center. Each linear polarization results in a phase-center calculation. Corresponding to this phase-center, there is a plot showing S21 phase variation with respect to the elevation angle. The high cost antenna has nearly constant S21 phase for each azimuth angle and polarization as opposed to the low-cost antenna for which the phase variation is greater. If the S21 phases are merged according to the discussion point 5 of the previous section (3.2), S21 phase for a circular polarization will result. Fig 3.5 shows that the S21 phase

variation for CP reception is nearly constant for the high cost antenna. The curves, therefore, show the variation in phase of the signal from a satellite as it passes over for several angles of rotation. Keep in mind, that this is the phase variation with respect to the (measured) phase-center. This may or may not be the designated point on the antenna where the location is assumed to be determined. It should be also mentioned that a plot of the magnitude of S21 for a given angle of rotation presents the classic radiation pattern of the antenna with respect to circular polarization. This has bearing if the magnitude at some angles becomes small thus making receiving of signals difficult.

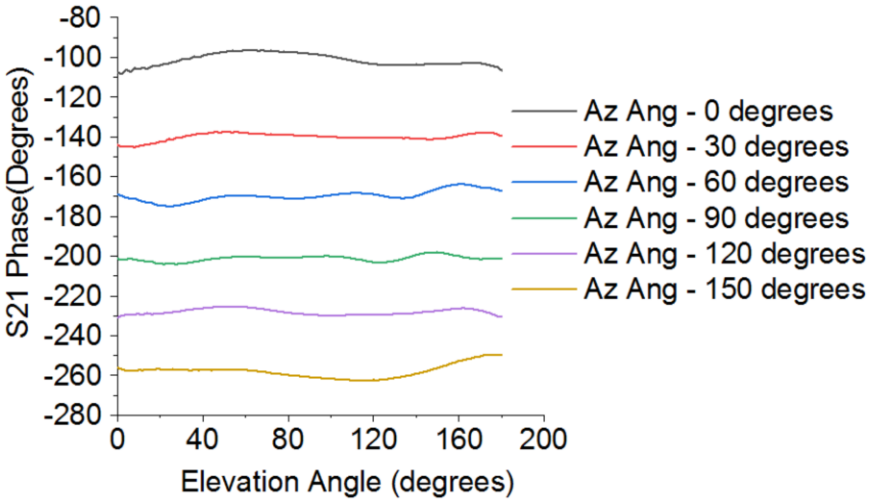

Figure 3.4 Variation S21 phase with respect to elevation angle for circular polarization and different azimuth angles for the high-cost antenna

It is observed that for the high cost antenna, the variation of the phase-center location is minimal and predictable as the azimuth angle changes. For the low-cost antenna, however, the phase-center motion is more erratic and cannot be predicted easily. Table 1 shows the phase-center positions for both the high-cost and low-cost antennas for each azimuth angle.

Table 3-1 Location of phase-center with respect to azimuth angle for both high cost and low cost antenna

Azimuth	**Low Cost antenna**			**High Cost antenna**		
	x(mm)	y(mm)	z(mm)	x(mm)	y(mm)	z(mm)
0	0	-4	9	7	5	55
10	0	-4	9	7	7	60
20	3	-4	9	8	7	60
30	7	-4	7	7	7	60
40	3	-6	6	5	7	60
50	3	-8	6	3	7	60
60	1	-2	6	0	5	60

70	1	0	6	0	3	60
80	0	2	4.5	-1	1	60
90	-4	-2	11.5	-2	-1	60
100	-18	-10	6	-3	-2	60
110	-18	-10	7	-3	-3	60
120	-18	-12	8	-4	-5	60
130	-20	-14	11	-5	-7	62.5
140	-18	-17	11	-6	-7	60
150	-16	-15	11	-8	-7	60
160	-12	-14	9	-12	-7	60
170	-10	-10	10	-10	-5	60
180	-10	-10	10	-8	-3	60

Fig. 3.5 shows 2D and 3D Matlab plots of data from Table 1 for the high cost antenna, whereas Fig. 3.6 shows 2D and 3D plots of data from Table 1 for the low cost antenna. A comparison of both figures shows that for the high cost antenna the points are more clustered. For the high cost antenna, the variation in the z-coordinate is minimal. The maximum X and Y variations are 20mm and 14mm respectively. For the low-cost antenna, the variation in z-coordinate is 7mm. The maximum X and Y variations are 27mm and 19mm respectively.

Fig 3.5 and Fig 3.6 below help give a sense of the spatial “ball” occupied by the phase-center. Obviously, the tighter the “ball,” the more accurate the location fixes will be. And it should be easier to find correction factors to accommodate the fact that the phase-center may not be at some assumed reference point on the antenna.

In any case, finding correction factors may not be straightforward. A simple approach would be to average the phase-center locations from each of the angles of rotation. This would give one point (x,y,z) which would be the approximate location as determined by the GNSS receiver. In general, the phase-center location varies with angle of rotation. If each satellite that was received passed over in a plane defined by an angle of rotation and if that angle could be estimated, then the phase-center for that plane could be used to determine a path length difference (from the assumed reference point) which, in turn, could be used to estimate the error in the time of arrival for the signal from that satellite. Unfortunately, a satellite trajectory over the receiver may not stay in a plane defined by a specific angle of rotation. It may cut across several thus experiencing a moving phase-center. Perhaps if the signal acquisition time is small enough, then some averaging of the variation of phase-center could be done provided the track of the satellite over the various angles of rotation could be estimated.

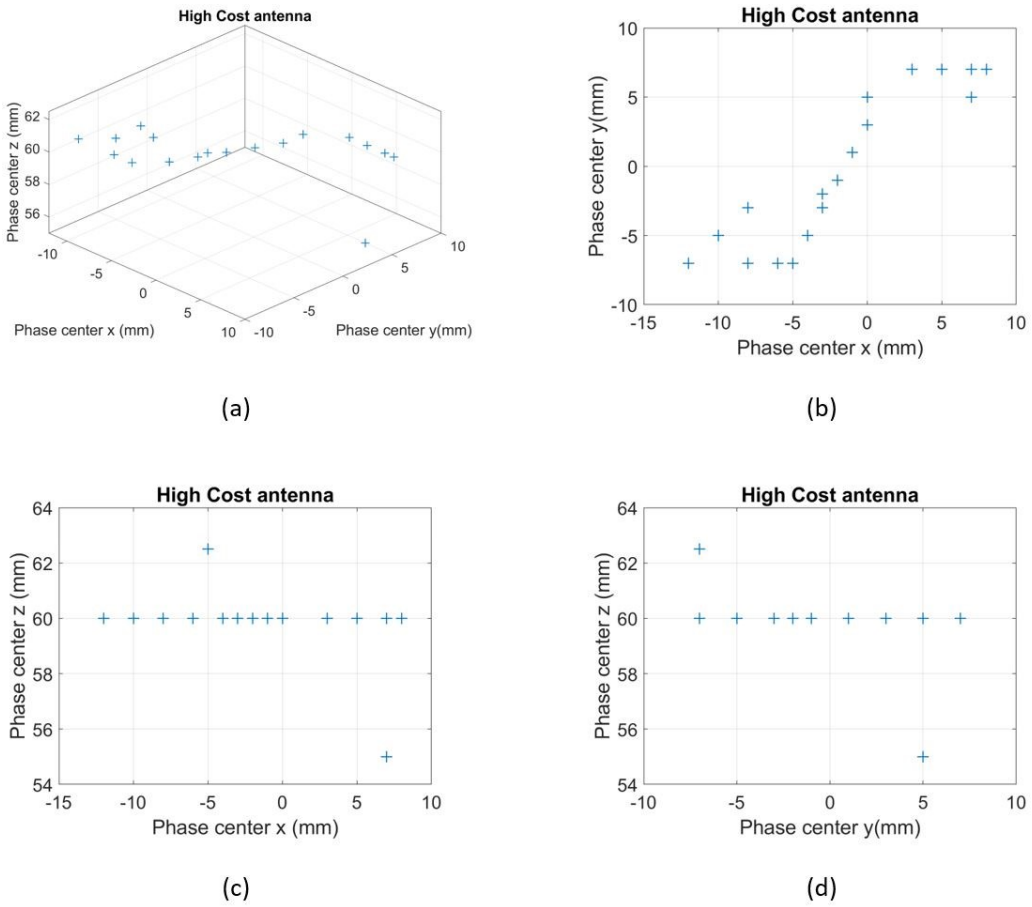

Figure 3.5 A set of 3D and 2D plots for phase-center variation of high cost antenna (a) 3D plot showing x, y and z locations of the phase-center for various azimuth angles in table 3.1 (b) 2D x-y plot (c) 2D x-z plot (d) 2D y-z plot

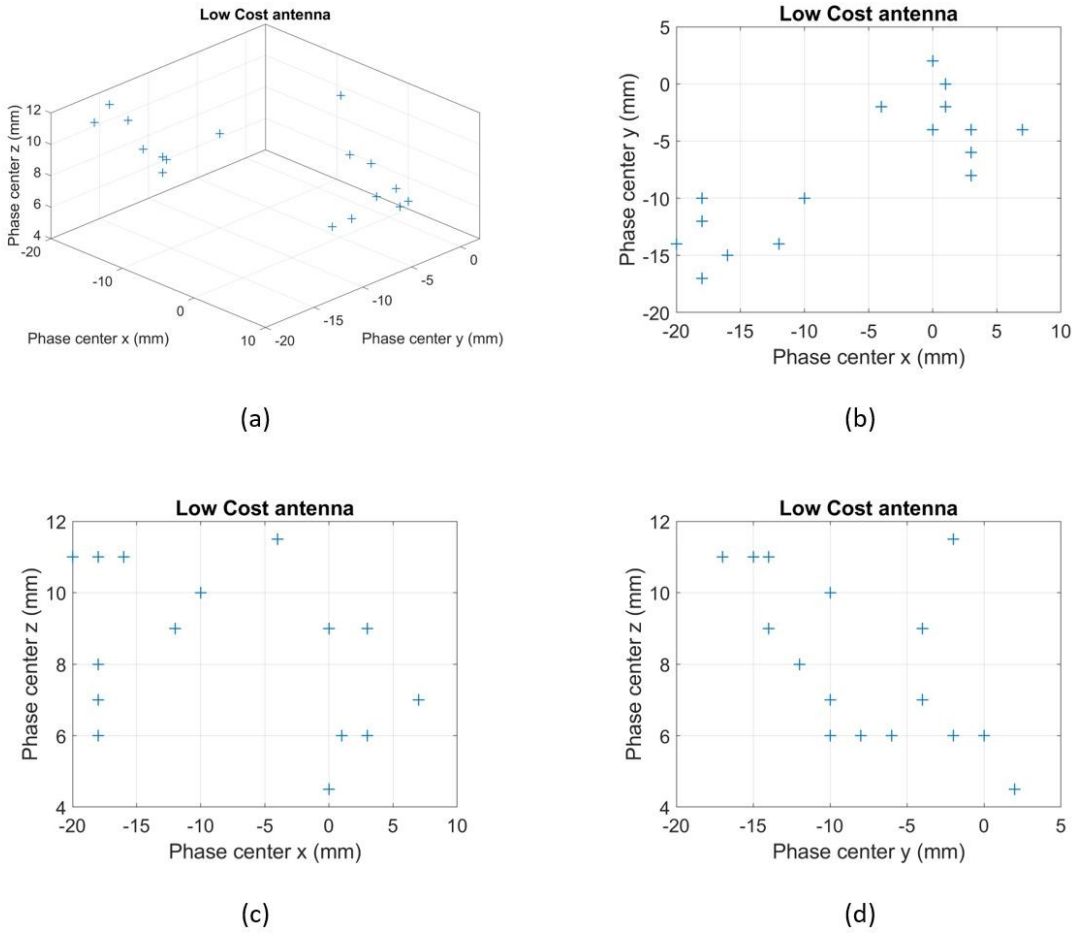

Figure 3.6 A set of 3D and 2D plots for phase-center variation of low-cost antenna (a) 3D plot showing x, y and z locations of the phase-center for various azimuth angles in table 3.1. (b) 2D x-y plot (c) 2D x-z plot (d) 2D y-z plot

CHAPTER 4: CONCLUSION AND SUGGESTED FUTURE WORK

The work in this report has shown that antenna phase-center motion has a non-negligible effect on the positioning solution of RTK (and by extension PPP). Given the above, more extensive evaluation of phase-center for low-cost antennas may be worthwhile to develop an understanding of how it varies with antenna type and the environment in which it is located. Although this probably requires extensive anechoic chamber work, perhaps some conclusions can be drawn about the phase-center variation "ball" that can be applied to ultimate obtainable location accuracies. As alluded to in section 3.3, another worthwhile task might be to develop an analytical approach to incorporating path-specific phase-center movement for each satellite (since it may be different depending on how the satellite passes over the receiver). This probably can be accomplished by modifying existing analytical approaches that are used to account for timing errors and a fixed (for all satellite paths) phase-center offset.

We are currently working on circularly polarized patch antenna designs to see how the specific design without the additional circuitry included in the commercial GPS designs will impact phase-error determination. These are being designed and will be fabricated and tested using the methods discussed for the anechoic chamber measurements. The aim will be to provide estimates for error range based on design type and connect this to the position-error information for which we currently have field measurements.

In view of the above, a promising approach may be to explore the possibility of gleaning information about antenna phase-center movement from GNSS observables. This appears to be possible for a high-quality antenna but perhaps not so for a low-quality antenna. The rationale for this is that it avoids expensive and time-consuming phase-center characterization in an anechoic chamber. An additional potential issue with a low-cost antenna is that its phase-center (and other characteristics) may vary depending on its immediate environment. Factors such as the size and shape of the structure the antenna is mounted on (or near to) may affect antenna performance since low-cost antennas usually do not have the electromagnetic isolation features that are part of a higher-cost antenna.

In what follows, we describe some preliminary work in using GNSS observables to estimate the effect of antenna phase-center motion. In this case, we use a pair of antennas in a differential mode in lieu of a single antenna. Thus, the effect we will observe or estimate is that of the combined phase-center motion of the antenna pair. As we will show, while some useful information can be gleaned from this, a usable model will require that the GNSS antennas be connected to receivers whose clocks are tied.

4.1 EXPERIMENTAL SETUP

Two Swift Navigation Piksi Multi GNSS receivers were utilized for the field data collection. Each receiver was connected to a single antenna. Two antennas were used for each test to allow for the "double differencing" of the incoming signals, thus allowing for the isolation of errors solely due to antenna properties. Each receiver was powered by a SigmasTek 12V SP12-100 NB car battery connected to an inverter. The batteries and electronics were housed in the weather-proof enclosure shown in Fig 4.1.

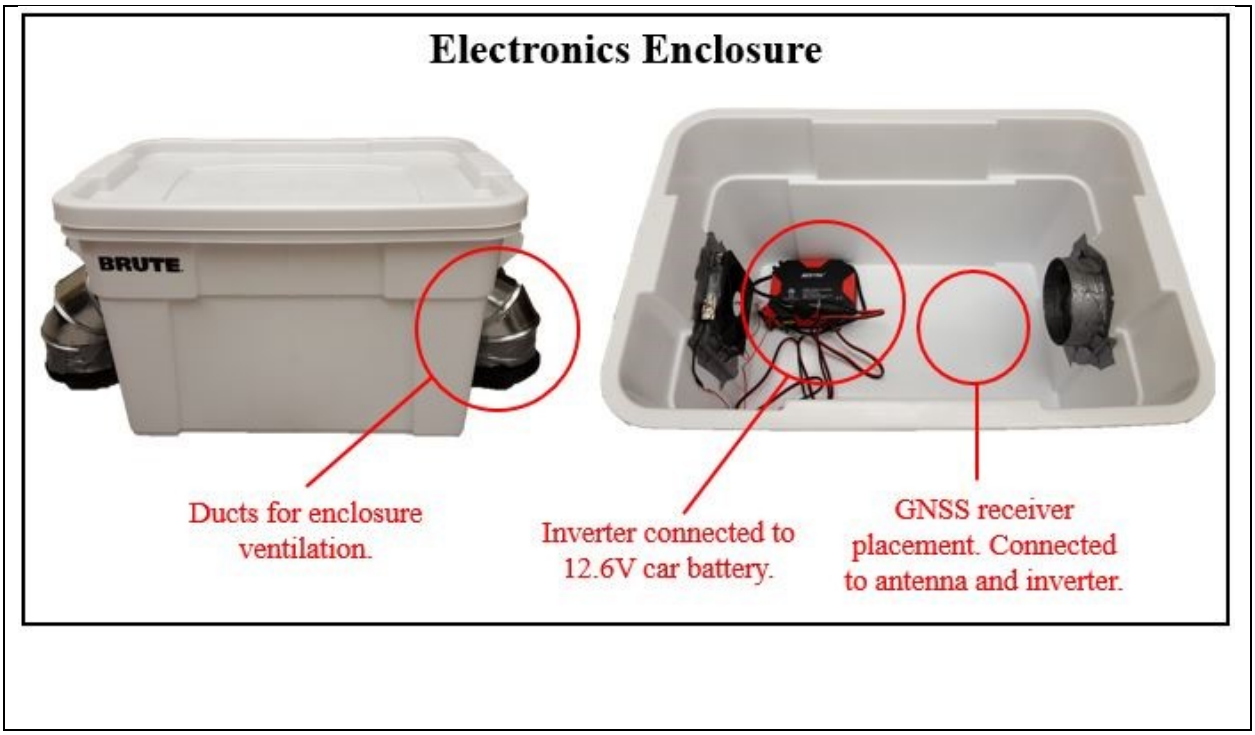

Figure 4.1 Overview of the electronics weather-proof enclosure used during field testing

Two antenna types were tested: a survey-grade antenna (NAVCOM ANT-3001R) and a low-cost patch antenna (uBlox ANN-MS). These were mounted on survey tripods located on top of, or in close proximity of, the DH4950 Minnesota Department of Transportation (MnDOT) geodetic marker in UMore Park, Rosemount, MN, shown in Fig. 4.2.

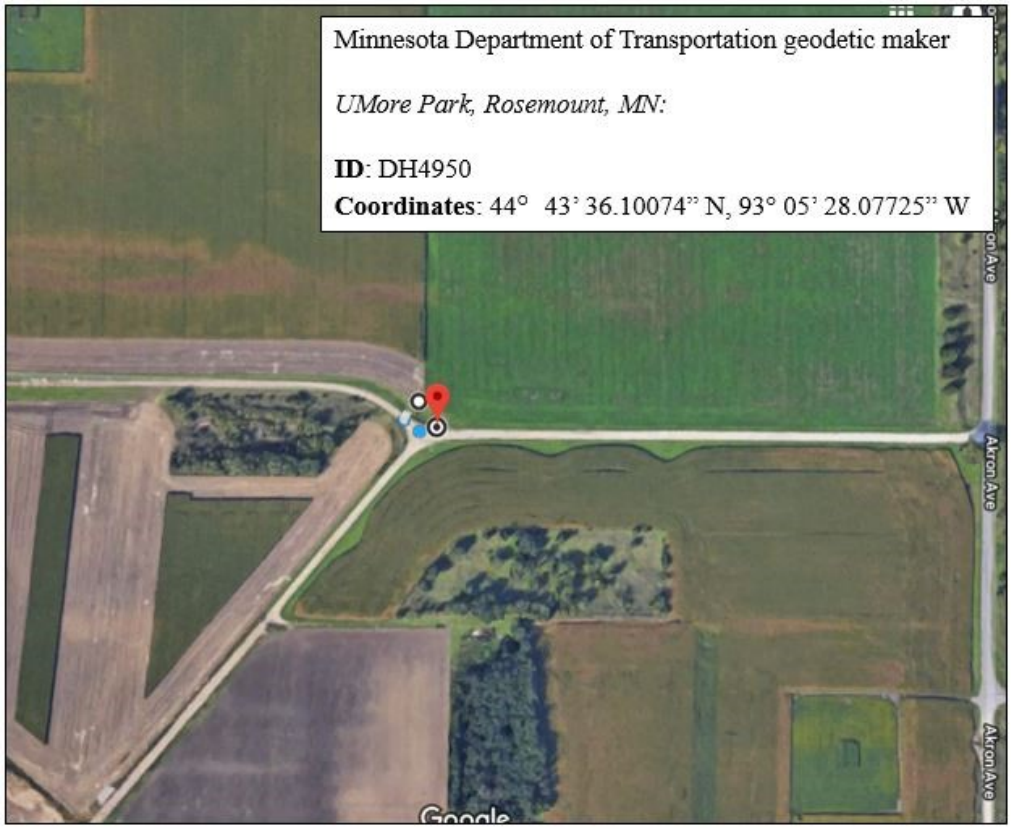

Figure 4.2 Satellite image, coordinates, and serial number of the geodetic marker utilized

The antennas where placed on a level surface at approximately the same height from the ground, pointing in the same direction, and separated by roughly $1\ m$. Fig. 4.3 and 4.4 outline the reference points used for the aforementioned setup for the uBlox ANN-MS and NAVCOM ANT-3001R, respectively. The diagrams

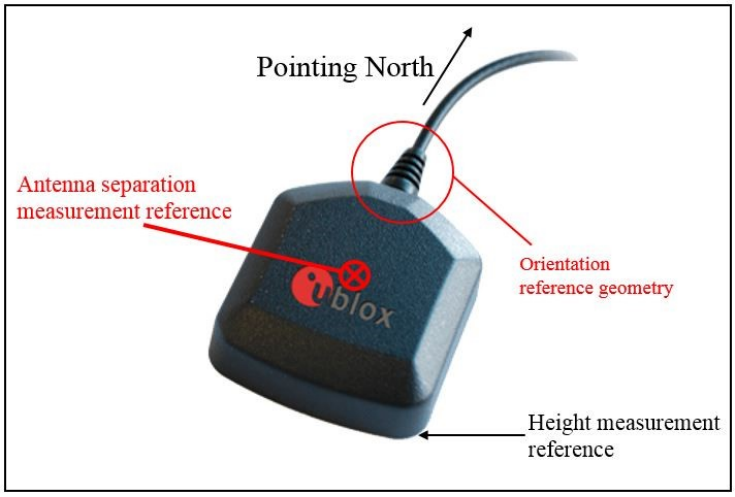

Figure 4.4 Reference points utilized for measurements with the uBlox ANN-MS

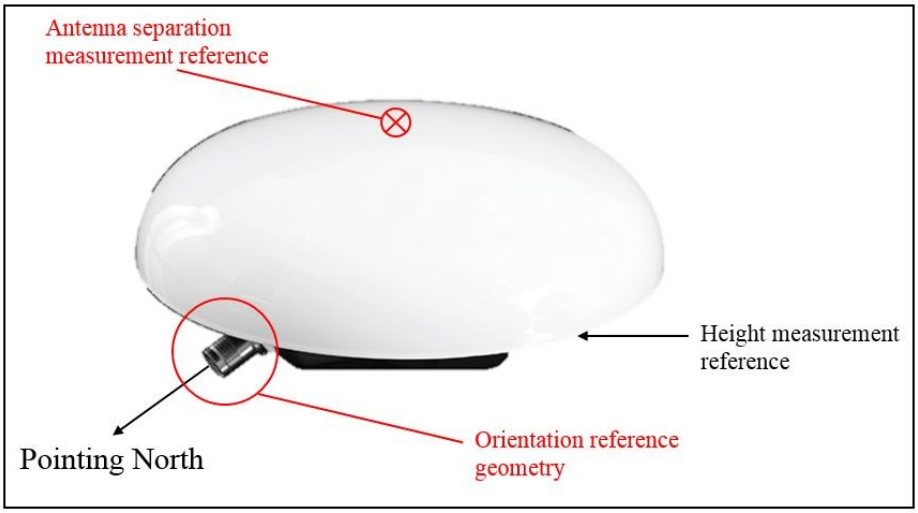

Figure 4.3 Reference points utilized for measurements with the NAVCOM ANT-3001R

show the reference geometry used to orient the antennas in the same direction, the reference point for separation measurements and the reference point for height measurements.

The placement of the antennas, relative to each other and relative to the geodetic marker, is outlined in Fig. 4.5 for their respective tests. Likewise, the separation between antennas, height from the ground, and the pictures of the experimental setup are included in Fig. 4.6. The same tripods, with different mounts for each antenna, are used during the tests. The data collection runs are also performed in similar weather conditions to maintain consistency between tests.

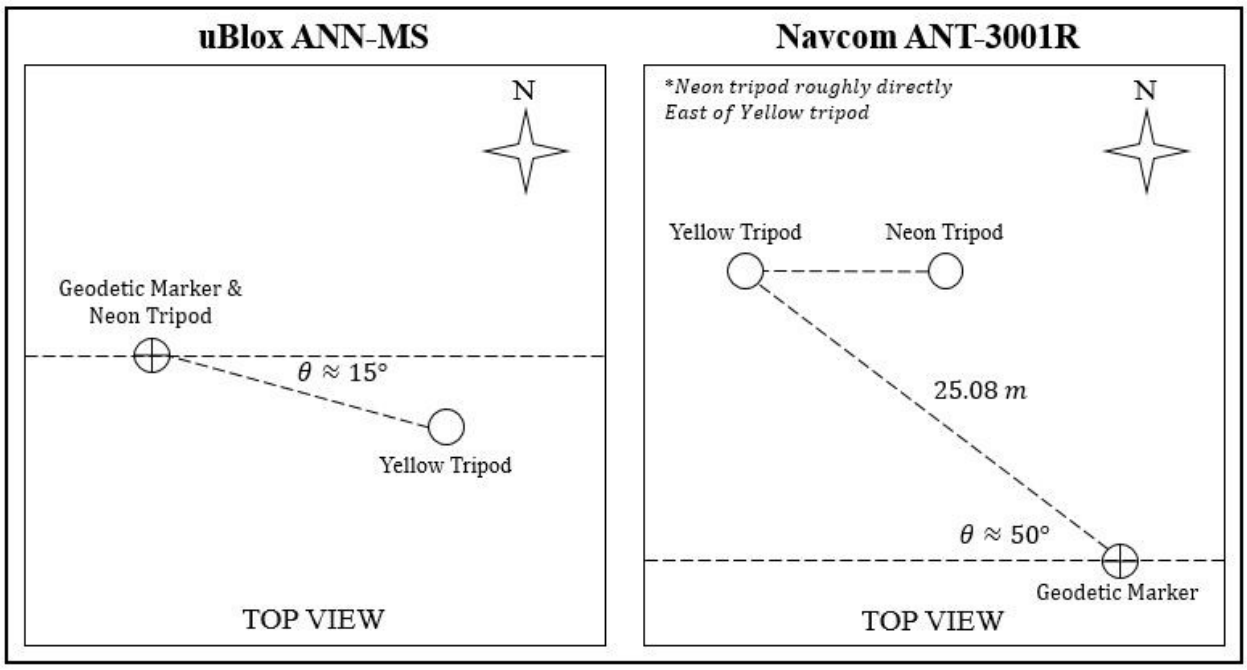

Figure 4.5 Relative placement of antennas, with respect to the geodetic marker and to each other, for each field test

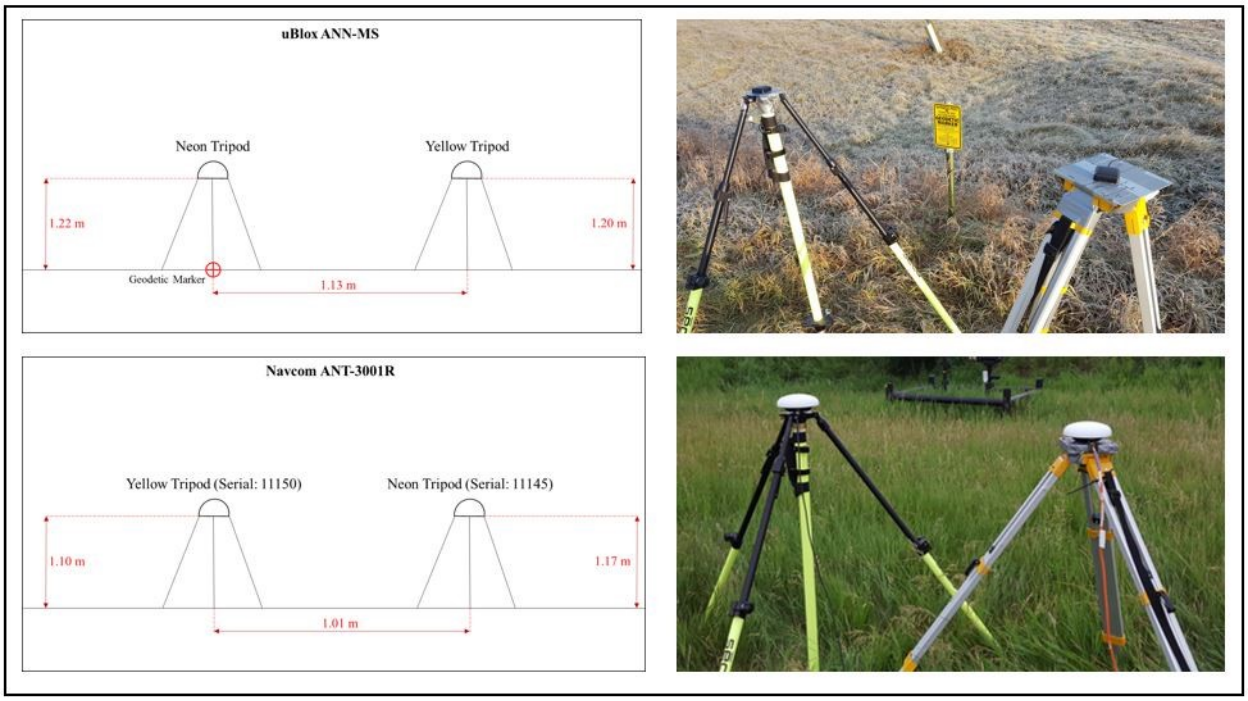

Figure 4.6 Separation of antennas from each other, and from the ground, for each field test

4.2 DATA ANALYSIS

Single difference (SD) was calculated based on the measurements collected for the high-quality and low-quality antennas. For high-quality antenna, Fig. 4.7 shows representative SD measurements (GPS satellite SV-9). We can see that SDs are bound between -30 to 30 cycles in magnitude. In contrast, a representative SD from low-quality antenna is shown. In this case, the data is for GPS SV-3. We see that this SD history has larger values in magnitude shown in Fig. 4.8. In addition, all the SD over 50 cycles are discarded when processing the raw measurements. From both Fig. 4.7 and Fig. 4.8, elevation and azimuth angle measurements change periodically as expected. The objective is to see if there is a strong correlation between SD and either elevation or azimuth angles. In other words, can we roughly estimate the magnitude of SD as a function of either elevation or azimuth angles? As was shown in Chapter 3, the phase-center variation is minimal for the high-cost antenna. This is also observed for the high-quality antenna in Fig. 4.7. Not only is the phase-center variation small, but its variation is also correlated with azimuth and elevation changes. For the low-cost antenna, the phase-center motion is more erratic and difficult to correlate with the azimuth and elevation changes. In what follows, we attempt to develop a more concrete correlation (functional relationship) between the line-of-sight geometry and the phase variation.

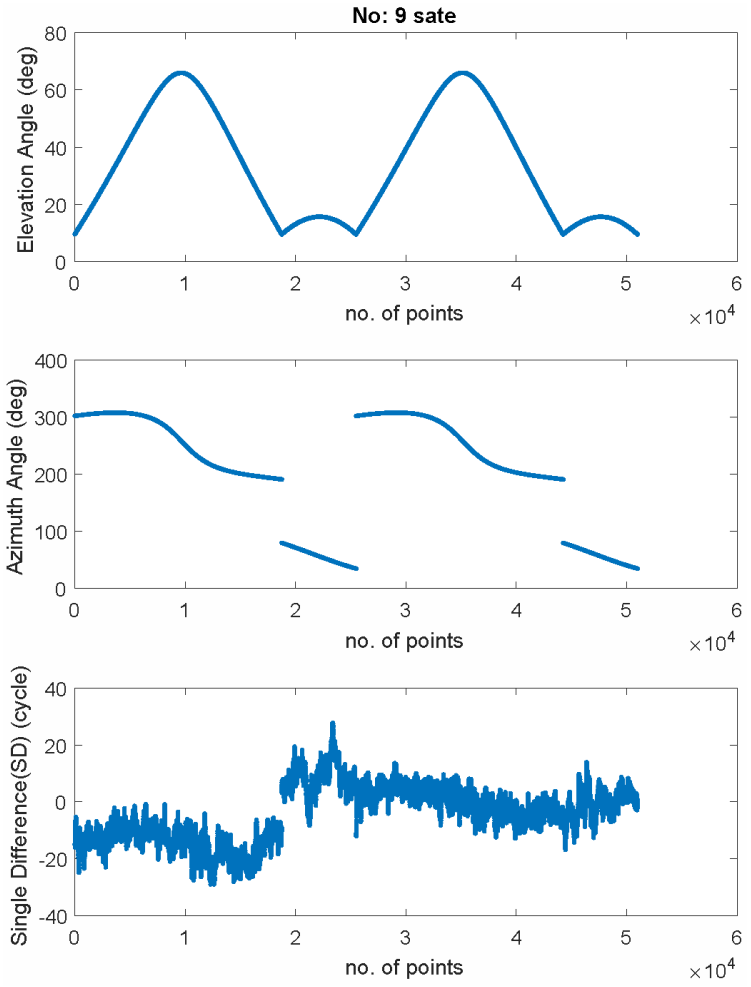

Figure 4.7 Sample single difference from GPS satellite #9 using high-quality antenna

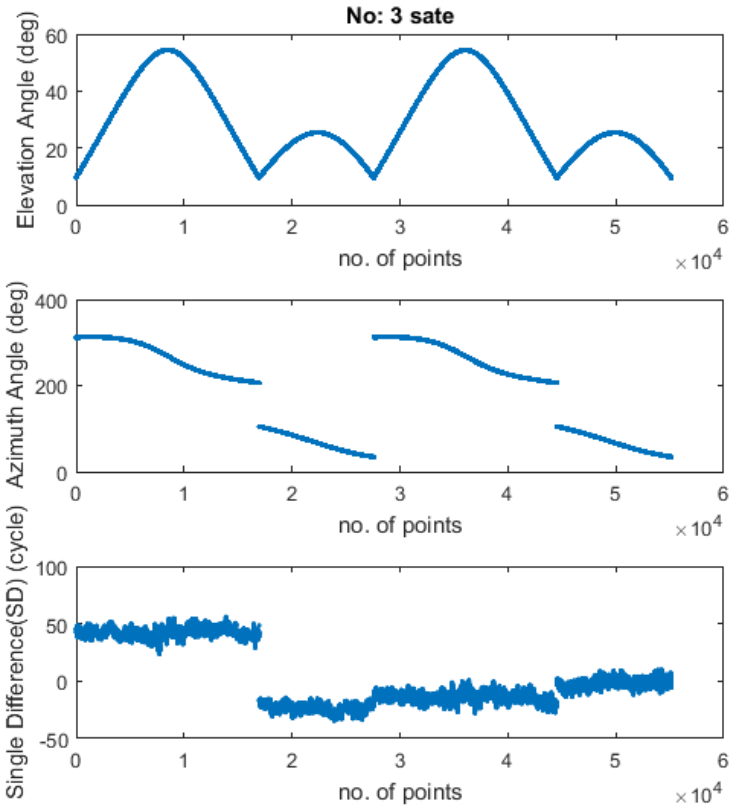

Figure 4.8 Sample single difference from GPS satellite #3 using lower-quality antenna

4.2.1 High-Quality Antenna

Given that the quality of the SD measurements is better for the high-cost antenna, we will start with it and try to determine the correlation between line-of-sight vector geometry and phase error. We plot the single difference (SD) versus azimuth angle using two sets of data in Fig. 4.9. It can be seen there is a clear trend in the SD across different azimuth angles. Using ideas from similar work described in [7], we fit this SD data with a 4th order polynomial model of the following form:

$$\nabla\varphi_{ab}^{k}(t) = \beta_0 + \beta_1\Lambda + \beta_2\Lambda^2 + \beta_3\Lambda^3 + \beta_4\Lambda^4$$

Variable Λ was the azimuth or elevation angle. In the analysis that follows, we found a stronger correlation between SD and azimuth angle. Thus, a fit with respect to azimuth angle was done. The resulting coefficients β_i are listed below in Table 4-1 .

Table 4-1. Fitting estimate for single difference

β_0	3.97	(3.773, 4.166)
β_1	-0.1089	(-0.1152, -0.1026)
β_2	-8.056e-05	(-0.0001453,-1.584e-05)
β_3	4.024e-06	(3.762e-06, 4.286e-06)
β_4	-8.541e-09	(-8.541e-09, -8.18e-09)

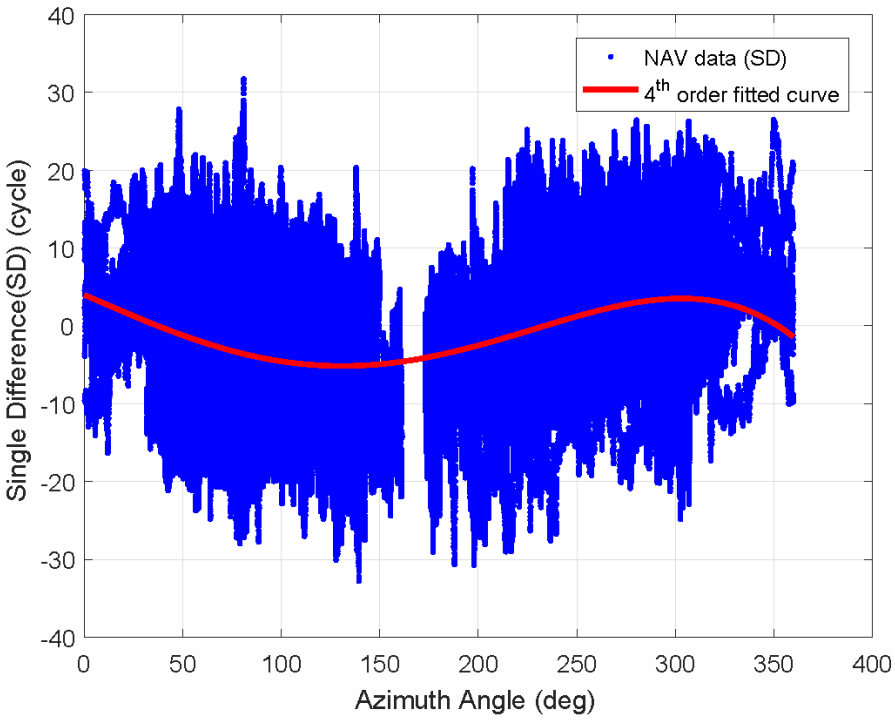

Figure 4.9 All single difference (cycle) versus azimuth angle (degree) from navigation survey grade antenna and its 4th polynomial fitting

As shown in the work of [7], we would expect to see an elevation dependence as well. However, this is not observed. One reason for this is that, in the work described, the clock of the two receivers were tied.

In our experiments, the two GNSS receivers ran on their own internal clocks. Thus, the SD residual error included the clock bias, which overwhelmed the phase-center errors. Thus, one of the messages from this is that estimation of phase-center motion errors from observed GNSS data should be done using receivers that run off the same clock.

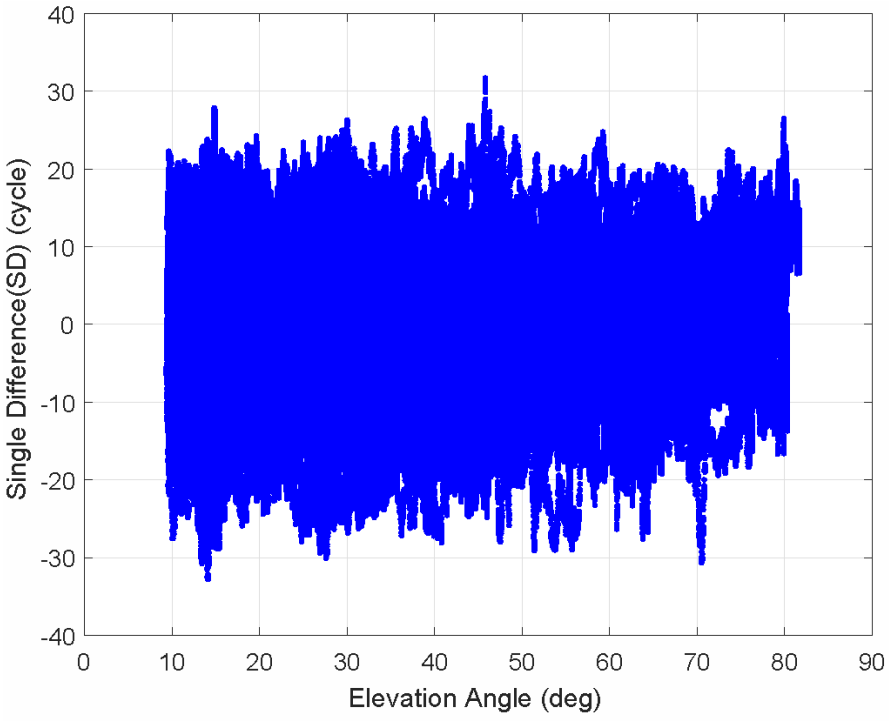

Figure 4.10 All single difference (cycle) versus elevation angle (degree) from low-cost antenna

As noted in Chapter 2, RTK is normally performed using double difference measurements instead of single difference measurements. Moreover, double differences remove the clock bias that is potentially corrupting the residuals seen in Fig. 4.9 and Fig. 4.10. Thus, we conducted a similar analysis using double differences. However, in this case, we need to be careful about what the line-of-sight geometry means. There is not clear meaning of azimuth and elevation in this case but rather differences. As such, we decided to select one satellite as the reference and use it as the base from which azimuth and elevation is measured. In other words, the boresight to the reference satellite is the datum relative to which measurements are being made. However, as shown in Fig. 4.11 and Fig. 4.12, this does not yield a discernable pattern relative to azimuth and elevation.

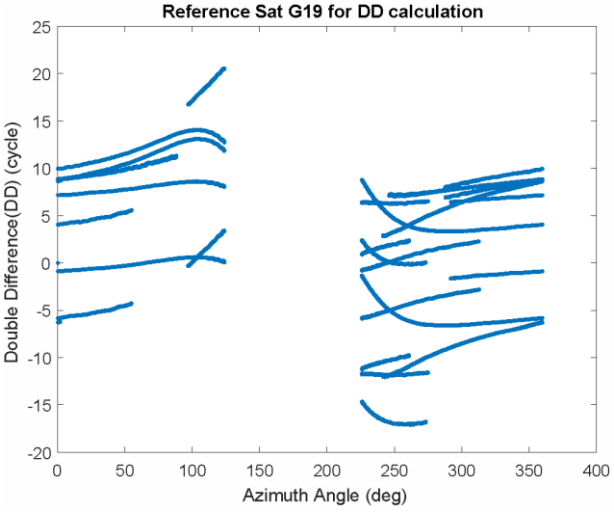

Figure 4.11 Double difference (cycle) vs. azimuth angle using GPS Satellite 19 as a reference

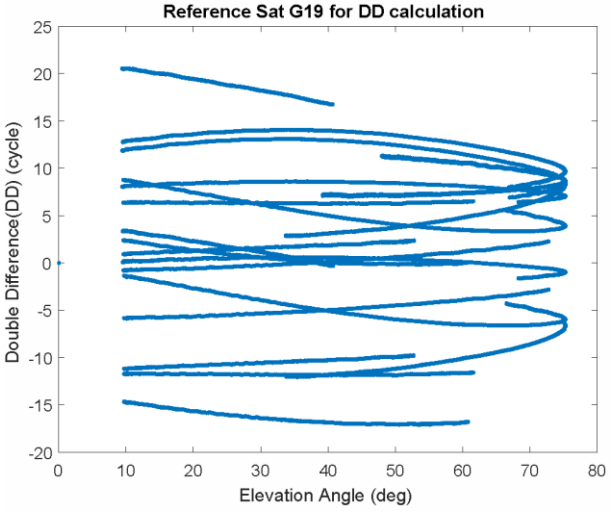

Figure 4.12 Double difference (cycle) vs. elevation angle using GPS Satellite 19 as a reference

4.2.2 Low-Quality Antennas

We repeated a similar exercise with the low-cost antennas. The single difference analysis is shown in Fig. 4.13 and Fig. 4.14. These plots show the single difference versus azimuth and elevation angle, respectively, using a low-quality antenna. Unfortunately, there is really no visual trend that can observed. Having a polynomial fit would not make any sense. It is inconclusive from both of these two figures. More work is needed to flush out a trend that will allow *in-situ* estimation of phase-center motion. This is the subject of ongoing work.

4.3 FUTURE WORK

While the analysis discussed above is not conclusive, it suggests that we can potentially estimate some of the phase-center variation errors provided we have access to data from a pair of GNSS antennas connected to a receiver or receivers driven by the same clock. At the moment, it is not clear how accurate an *in-situ* estimation scheme would be. However, if a few centimeters of phase-center variation can be modeled as a function of line-of-sight geometry or other parameters, it is clear that a small improvement in the RTK and PPP solutions can be achieved. This is the subject of on-going work.

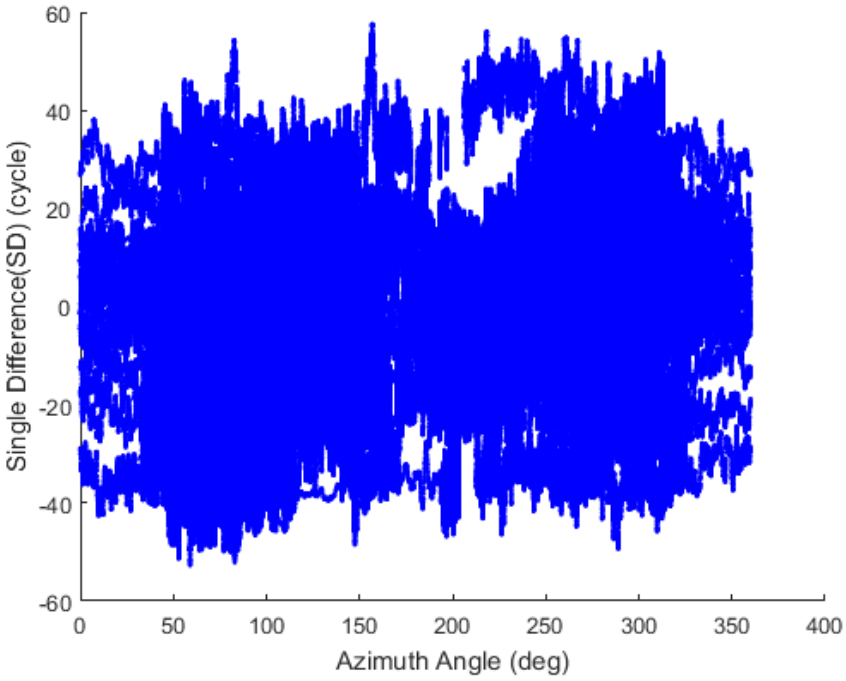

Figure 4.13 All single difference (cycle) versus azimuth angle (degree) from low-grade antenna

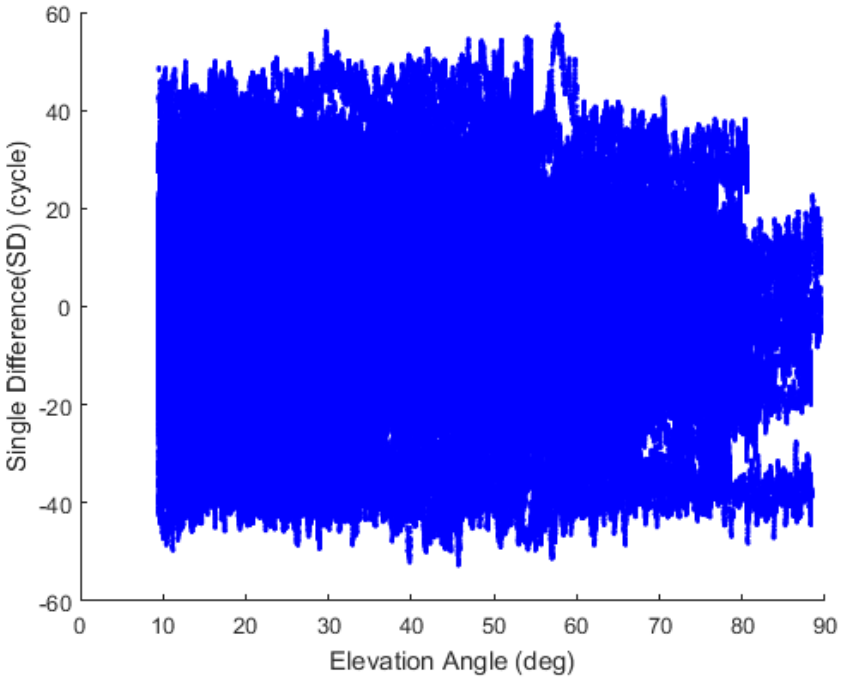

Figure 4.14 All single difference (cycle) versus elevation angle (degree) from low-grade antenna

REFERENCES

[1] P. Misra & P. K. Enge. (2010). *Global Positioning System: Signals, Measurements, and Performance,* Second ed. Boston: Ganga-Jamuna Press.

[2] A. Prata. (2002). Misaligned antenna phase-center determination using measured phase patterns (IPN Progress Report 42-150). Pasadena, CA: Interplanetary Network, Jet Propulsion Laborary, California Institute of Technoloby.

[3] W. Kunysz. (2010). Antenna phase center effects and measurements in GNSS ranging applications. In *14th International Symposium on Antenna Technology and Applied Electromagnetics & the American Electromagnetics Conference*, Ottawa, Ontario.

[4] Navcom. (2009). ANT-3001R, ANT-3001A, ANT-3001BR datasheet. Retrieved from https://www.navtechgps.com/assets/1/7/Navcom_Antennas_DS.pdf.

[5] u-blox. (2017). ANN-MS Active GPS antenna datasheet. Retrieved from https://www.ublox.com/sites/default/files/ANN_DataSheet_%28UBX-15025046%29.pdf.

[6] C.-S. Y.-J. C. a. T.-K. Y. Chen. (2000). The impact of GPS antenna phase center offset and variation on the positioning accuracy. *Chen, Chun-Sung, Bollettino di Geodesia e Scienze Affini, 59*(1), 73–94.

[7] G. Zheng. (2010). *Methods for Enhancing Carrier Phase GNSS Positioning and Attitude Determination Performance*. Minneapolis, MN: University of Minnesota.